Enantioselective fullerene functionalization through stereochemical information transfer from a self-assembled cage

Zifei Lu, Tanya K Ronson, Andrew W Heard, Sascha Feldmann, Nicolas Vanthuyne, Jonathan R Nitschke

Enantioselective fullerene functionalization *via* traceless stereochemical information transfer from a self-assembled cage

AUTHORS

Zifei Lu[1], Tanya K. Ronson[1], Andrew W. Heard[1], Sascha Feldmann[2], Nicolas Vanthuyne[3], Alexandre Martinez[3], Jonathan R. Nitschke*[1]

[1]Yusuf Hamied Department of Chemistry, University of Cambridge, Lensfield Road, Cambridge, CB2 1EW, United Kingdom

[2]Cavendish Laboratory, University of Cambridge, J J Thomson Avenue, Cambridge, CB3 0HE, United Kingdom

[3]Aix Marseille University, CNRS Centrale Marseille, iSm2, 13284 Marseille, France

Metal-organic cages have served as masks to effect the regioselective functionalization of C_{60}. The enantioselective functionalization of C_{60} remains challenging, however, requiring complex chiral tethers or challenging chromatography. We report a means of defining up to six stereocentres on C_{60}, achieving both enantioselective and regioselective fullerene functionalisation. This method involves stereochemical information transfer from a chiral formylpyridine, through the framework of an enantiopure cage incorporating it, to a series of regio- and stereochemically defined C_{60} adducts. The surrounding cage is then opened with retention of fullerene stereochemistry. The chiral formylpyridine thus ultimately dictates the stereochemistry of these chiral fullerene adducts without being incorporated into them. The cage acts both as the substrate and "blueprint" for the chiral information imprinted into the fullerene adducts, which form stereoselectively with a distance of up to 6 carbon atoms between stereocentres. Such chiral fullerene adducts may become useful in devices requiring circularly-polarized light manipulation.

INTRODUCTION

The flow of stereochemical information is integral to the processes of life, such as the recognition of steroids and saccharides by receptors, and the stereospecific transformations of substrates by enzymes. Stereochemical communication is likewise central to elegant artificial processes[1], which include extraordinarily remote stereocontrol through foldamer chains[2–4], the transduction of rotatory motion from molecular motors up to the macroscopic scale[5], and the creation of valuable pharmaceuticals through organocatalysis[6].

Many metal-organic cages are chiral, with stereochemistry controlled through the use of enantiopure ligands prepared through multi-step organic synthesis and preparative chiral HPLC[7–9]. Alternatively, chiral counterions, chiral amines[10] or auxiliary ligands[11] have enabled stereoselective cage construction. In recent years several elegant examples of asymmetric recognition and catalysis within the chirotopic cavities[12] of enantiopure cages have been reported[13–15]. However, achieving these functions remains challenging due to the pseudo-spherical nature of the voids in high-symmetry molecular cages, which makes it difficult for them

to differentiate between enantiomers of chiral guests. New strategies are thus needed, both to control the stereochemistry of cages and to put their chirality to practical use.

Aromatic panelled metal-organic cages have been shown to be excellent hosts for fullerenes[16–19] and have been used to control their regioselective functionalization, through confinement effects[20] or by acting as a supramolecular mask[21–24] to control the sites of substrate addition. Such functionalised fullerenes are of interest due to their applications in optoelectronics, medicine, and materials science[25–27]. Their development has been hampered by the difficulty of selective multiple functionalisation of the spherical fullerene core and challenges associated with separation of the desired fullerenes by column chromatography or by high performance liquid chromatography (HPLC)[28,29]. Less use has thus been made of enantiopure fullerenes than would otherwise have been the case, despite the promise they show in chiral induction of polymers[25], peptide synthesis[26] and the detection of circularly polarized light (CPL)[27]. Their construction has relied on bulky, permanently-attached tethers, chiral HPLC, or lengthy synthetic procedures[29–31]. Chiral derivatives of C_{60} fall into two main categories: those with functionalization patterns that are not inherently chiral, but that possess stereocentres in their substituents, and those with inherently chiral functionalization patterns, having chirality induced by the geometric arrangement of addends. This second category is particularly challenging to access without the use of challenging chiral HPLC separations or chiral auxiliaries to aid purification. A larger steric difference between stereoisomers may be observed, however, when chirality results from the geometric arrangement of addends, rather than remotely attached on the substituents, adding interest to this second group of fullerene adducts[32].

Here we report the synthesis of an enantiopure metal-organic cage, whose stereochemistry is defined through the incorporation of a chiral formylpyridine subcomponent. This cage reacts with the fullerenes C_{60} and [6,6]-Phenyl-C61-butyric acid methyl ester (PCBM) *via* chemo-, regio- and enantioselective Diels-Alder cycloaddition with the anthracene panels of the cage. The resulting enantioenriched homo- and hetero-substituted fullerenes may be readily cleaved from the cage, without the need for challenging and costly HLPC purifications. These fullerenes have inherently chiral functionalization patterns, but contain none of the initial chiral formylpyridine, which may be recovered following cage disassembly, as with organic chiral auxiliaries[33,34]. Optical spectroscopy confirms the existence of an excited state with a microsecond lifetime for one of the adducts, which we assign to a triplet exciton carrying net spin. Together with the observed circular dichroism, this long-lived excited state renders the reported family of materials promising candidates for future optoelectronic applications exploiting chirally-induced spin-selectivity[35].

RESULTS AND DISCUSSION

Enantiopure formylpyridine subcomponent **A** (Fig. 1a) was synthesized through a three-step process in 81% overall yield (Supplementary Scheme S1), with the aim of using it to shape the stereochemistry of new cage complexes. Whereas chiral amines had been incorporated into cage frameworks[10], chiral aldehydes have not yet been used to control the handedness of metallosupramolecular constructs prepared through subcomponent self-assembly. The development of a chiral aldehyde greatly extends the range of cages that can be prepared in enantiopure form, including cages made with more enclosed panels that provide the larger

cavities known to have good binding properties, enabling their chirality to be put to use. Additionally, cages based on multi-topic amine cage subcomponents may be conveniently decomposed with treatment with tris(2-aminoethyl)amine. A chiral 1-phenylethanol unit was installed in the 3-position of the pyridine ring of **A** to ensure its proximity to the metal centre while avoiding steric clash around the coordination sphere of the metal ion, which could destabilise subsequent assemblies. With the two enantiomers of **A** in hand, we set out to explore the stereochemistry of cages that form from it *via* subcomponent self-assembly.

Self-assembly with linear terphenyl subcomponent B

The reaction of linear terphenyl subcomponent **B** with 2-formylpyridine and iron(II) was shown to produce a mixture of homochiral *T* (ΛΛΛΛ/ΔΔΔΔ), heterochiral C_3 (ΔΔΔΛ/ΛΛΛΔ), and achiral S_4 (ΛΛΔΔ) $Fe^{II}_4L_6$ cage diastereomers[36]. We thus investigated the degree of stereocontrol that chiral subcomponent **A** might engender within an analogous tetrahedral cage framework incorporating **B** residues. The reaction between (*R*)-**A**, **B** and iron(II) trifluoromethanesulfonimide (triflimide, NTf_2^-) yielded $Fe^{II}_4L_6$ cage **1** (Fig. 1a), as confirmed by ESI-MS (Supplementary Fig. S15). The ^{1}H NMR and ^{13}C NMR spectra of **1** (Supplementary Figs. S8 and S11) were complex, exhibiting clusters of peaks. All ^{1}H NMR peaks between 4.50 and 9.50 ppm displayed a single diffusion constant in ^{1}H DOSY NMR (Supplementary Fig. S14), consistent with the presence of multiple diastereomeric species having the same size.

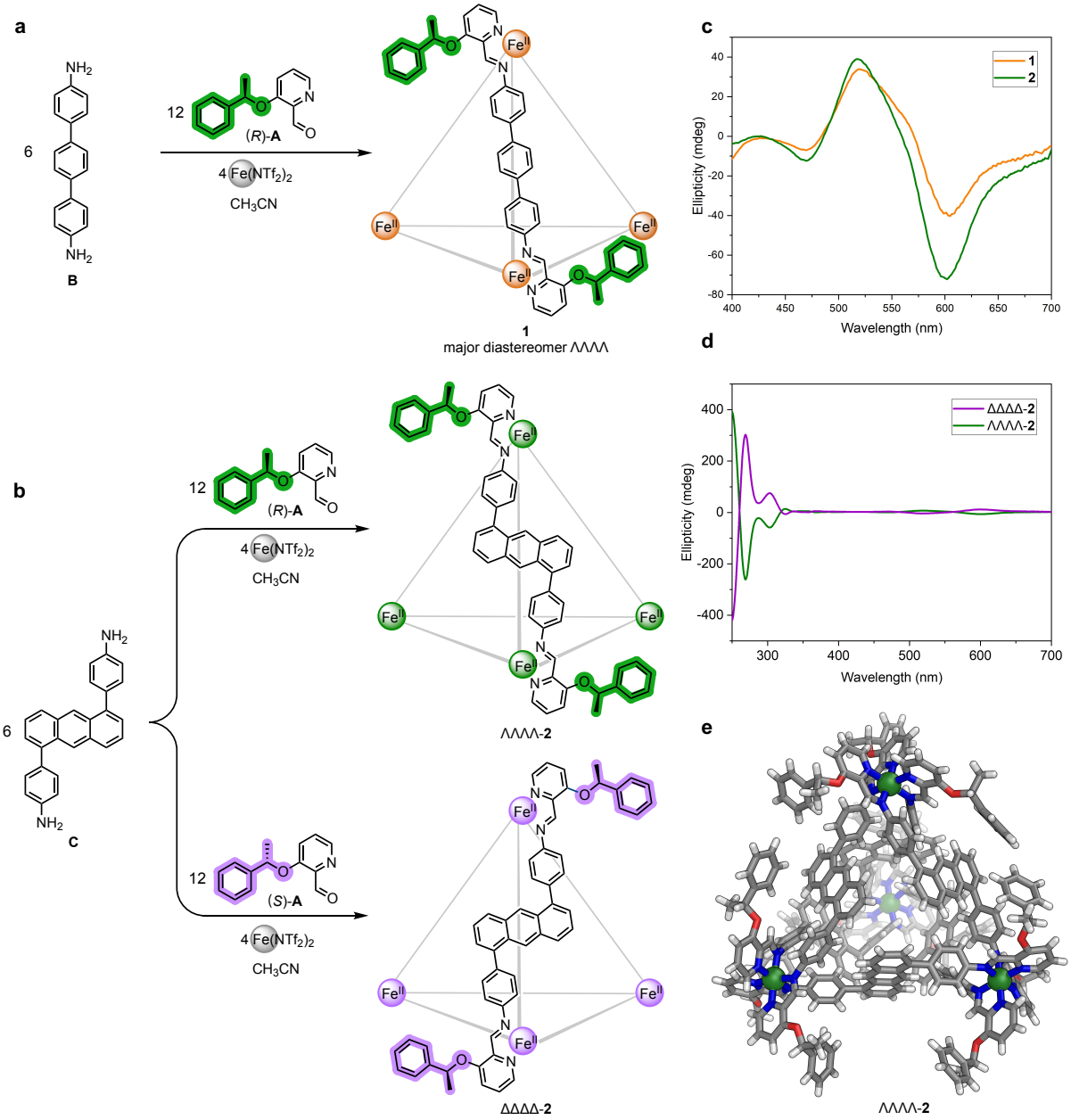

Fig. 1 | Preparation and characterization of cages 1 and 2. a, Synthesis of cage **1** from (*R*)-**A** as a mixture of diastereomers; only the majority *T*-symmetric diastereomer is shown. **b,** Synthesis of enantiomeric cages ΛΛΛΛ-**2** and ΔΔΔΔ-**2** from (*R*)-**A** and (*S*)-**A**, respectively. **c,** Comparison of the CD spectra of cages **1** and ΛΛΛΛ-**2** (MLCT region shown, data normalized to the UV-Vis absorption at the MLCT maxima at 585 nm for **1** and **2**,). **d,** CD spectra of the two enantiomers of cage **2**. **e,** X-ray crystal structure of ΛΛΛΛ-**2** (Fe^{II}, green; C, grey: N, blue; O, red; H, white, solvent of crystallization and anions omitted for clarity).

Examination of the imine region of the ^{1}H NMR spectrum of **1** revealed a major peak assigned to the *T*-symmetric diastereomer, comprising 50% of the integrated imine intensity (Supplementary Fig. S9). This observation is consistent with a 1.5-fold increase in preference for this diastereomer relative to the unsubstituted cage, where an approximately equimolar mixture of the three diastereomers had been

observed[36], already reflecting a slight preference for the *T*-symmetric diastereomer as compared to a statistical distribution of 12.5% *T*, 50% C_3 and 37.5% S_4.

The incomplete stereochemical induction in **1** was attributed to the limited ability of dianiline **B** to transmit stereochemical information between vertices. We had previously hypothesised that cages incorporating such linear dianilines exhibited weaker stereochemical coupling between metal-centre vertices as compared to bis(2-formylpyridine)-based cages because of the lack of offset between metal-binding sites within the subsequently formed imine ligand[37]. Such dianiline-based cages exhibit less distortion of the ligands when mixtures of *syn*- and *anti*- ligands are incorporated into the C_3 and S_4 diastereomers, and thus a decreased preference for the *T* diastereomer where all ligands adopt the *anti*-conformation. The moderate degree of chiral induction observed in **1** prompted us to explore the chiral induction of (*R*)-**A** with aniline subcomponents having a greater degree of offset, which has been shown to lead to a higher degree of stereochemical coupling between metal-ion vertices[38].

Self-assembly with 1,5-anthracene-containing subcomponent C

Dianiline subcomponent **C**, which contains a 1,5-anthracene spacer, was previously shown to form only the homochiral *T* (ΛΛΛΛ/ΔΔΔΔ) diastereomer, upon self-assembly with $Fe(NTf_2)_2$ and 2-formylpyridine[38]. The self-assembly of **C** (6 equiv) and enantiopure formylpyridine (*R*)-**A** (12 equiv) with $Fe(NTf_2)_2$ (4 equiv) yielded $Fe^{II}_4L_6$ cage **2**, as confirmed by ESI-MS (Fig. 1b and Supplementary Fig. S28).

The ^{1}H NMR spectrum of cage **2** showed a single set of peaks (Supplementary Fig. S22), indicating the selective formation of a single diastereomer. The circular dichroism (CD) spectrum of ΛΛΛΛ-**2** contains negative exciton-coupled circular dichroism (ECCD) couplets around 550 nm (Fig. 1d and Supplementary Fig. S33) which correspond to the metal-to-ligand charge-transfer (MLCT) bands for Fe^{II} pyridyl-imine complexes, indicating a single handedness of Λ metal stereocentres[10]. The solid-state structure of cage ΛΛΛΛ-**2** was determined by single crystal X-ray diffraction analysis (Fig. 1e). This crystal structure confirmed Λ handedness for all four metal centres.

The Λ helicity of the metal stereocentres seen in the crystal structure of **2** agree with the intense ECCD couplet from coupling of the π–π* transitions in the imine chromophores seen in the CD spectrum indicating the selective formation of the ΛΛΛΛ isomer in solution[39]. The enantiomeric cage ΔΔΔΔ-**2** was also prepared, starting from (*S*)-**A**, and the CD spectra of both cages appear with exact mirror symmetry (Fig. 1d).

The CD and UV-vis absorption spectra of cages **1** and ΛΛΛΛ-**2** are very similar in the MLCT region (400-700 nm). We thus compared the MLCT CD signals of cages **1** and ΛΛΛΛ-**2**, in both cases normalising the CD intensity to the corresponding maximum UV-vis absorption intensity in the MLCT region (Fig. 1c). This comparison provides insight into the degree of stereochemical coupling between the chiral aldehyde residues and the metal stereocentres within cage **1**. The proportion of ellipticity θ(**1**)/θ(**2**) is calculated to be 0.67, indicating the presence of significant chiral induction within cage **1** despite its diastereomeric diversity. Most of this CD signal is inferred to derive from the majority ΛΛΛΛ *T* diastereomer, which gives rise to the single

major peak (50% of the integrated intensity) in the imine region of the ^{1}H NMR of cage **1** noted above. Further discussion can be found in Supplementary Information Section 2.2.

Thus, new formylpyridine (*R*)-**A** was shown to render cage **2** enantiopure, but to have a more limited influence over the stereochemistry of cage **1**.

Synthesis of chiral fullerenes *via* traceless stereochemical information transfer from enantiopure cage 2

Anthracene panels in the racemic analogue of cage **2** have been shown[38] to undergo diastereoselective Diels–Alder reaction with C_{60}, where three anthracene panels were observed to react with the fullerene. We hypothesized that enantiopure **2** would also react with C_{60}, potentially fixing the precise stereochemistry of six carbon stereocentres in a single enantioselective process.

The reaction between cage **2** and excess C_{60} (5 equiv) in acetonitrile did indeed result in the formation of a new 1:1 adduct, with the stoichiometry confirmed by ESI-MS (Supplementary Fig. S43). Due to the insolubility of C_{60} in acetonitrile, we could not quantify the binding strength in cage **2**. The six C–C bonds formed during binding imply a high association constant. ^{1}H NMR spectroscopy (Supplementary Fig. S35) allowed us to assign the major peaks (ca. 95%) to four magnetically distinct environments of equal intensity for each proton type, consistent with the formation of a product with C_3 symmetry.

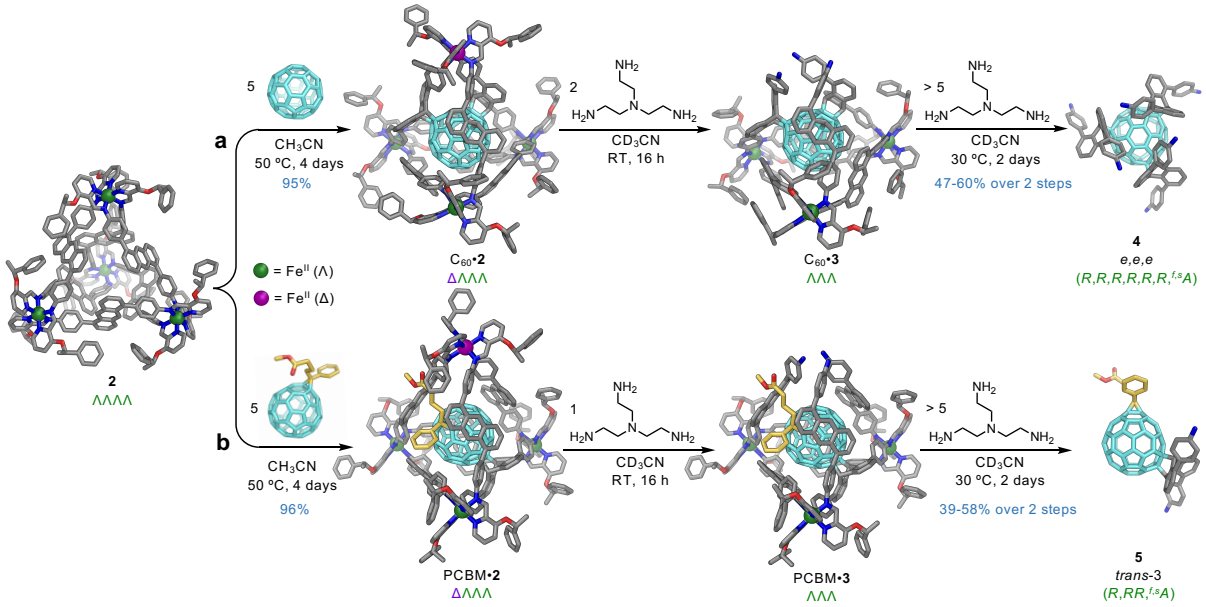

Fig. 2 | Reaction of cage 2 with C_{60} and PCBM. a, Cage **2** reacted stereoselectively with C_{60}, resulting in the formation of an adduct with six new stereocentres having defined stereochemistry. **b,** The reaction between **2** and PCBM stereoselectively formed an adduct with two new stereocentres on separate hemispheres of C_{60}. In both cases, stepwise addition of *tren* resulted first in removal of the apical metal centre, followed by complete disassembly to yield the final fullerene adducts. Cages **2** and C_{60}•**2** are shown as their X-ray structures; all other structures are models produced with SCIGRESS, hydrogen atoms are omitted for clarity.

The crystal structure of ΔΛΛΛ-C_{60}•**2** confirmed the formation of a covalent Diels–Alder adduct between ΛΛΛΛ-**2** and C_{60} (Fig. 3a). The fullerene is centred within the $Fe^{II}_4L_6$ cage, having reacted with three of the six anthracene panels. The three anthracene ligands that have undergone cycloaddition share an apical vertex of the cage, producing a C_3-symmetric configuration consistent with solution NMR spectra. Despite the preference for a Λ metal configuration, which the (*R*)-**A** derivative was demonstrated to induce, the handedness of the apical Fe^{II} centre of C_{60}•**2** was observed to invert following reaction, as was also observed in its racemic analogue[38].

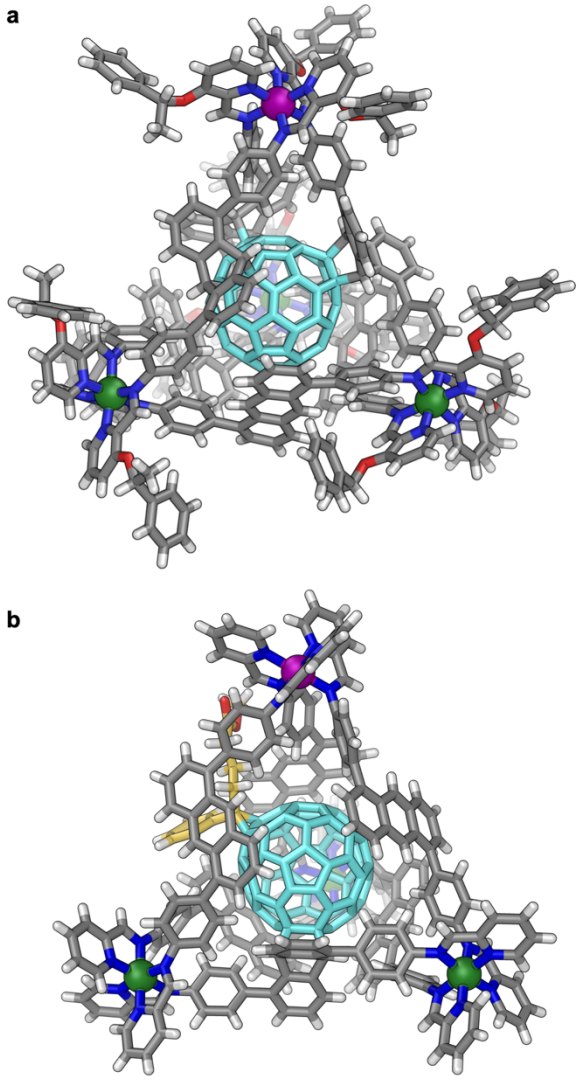

Fig. 3 | X-ray crystal structures of cages ΔΛΛΛ-C_{60}•2 and PCBM•2'. a, Three anthracene panels per cage have reacted with C_{60} in ΛΛΛΛ-C_{60}•**2**, lending the structure C_3 symmetry. **b**, One anthracene panel per cage has reacted stereoselectively with PCBM in PCBM•**2'** (carbons on the side chain of PCBM coloured yellow; both ΔΛΛΛ and ΛΔΔΔ enantiomers are present in the unit cell but only the ΔΛΛΛ enantiomer of PCBM•**2'** is shown here for clarity). In both cases Δ and Λ metal centres are coloured purple and green respectively and the fullerene carbon atoms are cyan. Solvents, counterions and disorder are omitted for clarity. See Supplementary Information Section 6 for a full discussion of fullerene reactivity.

Encouraged by the diastereoselective reaction observed with C_{60}, we investigated the Diels–Alder reaction of cage **2** with the opto-electronically important[27], singly-functionalised C_{60} derivative PCBM under identical reaction conditions. ESI-MS confirmed the formation of a 1:1 adduct (Supplementary Fig. S62). In contrast to the C_3 symmetry reflected in the ^{1}H NMR spectra of C_{60}•**2**, the PCBM•**2** adduct displayed complete desymmetrisation, with all protons in magnetically distinct environments (Supplementary Fig. S55).

Although numerous attempts to obtain X-ray quality crystals of PCBM•**2** were unsuccessful, we were able to obtain the crystal structure of its racemic analogue PCBM•**2'**, which was synthesized by treating PCBM with cage **2'**, an analogue of cage **2** prepared using 2-formylpyridine in place of chiral (*R*)-**A**, which was previously reported by our group[38]. Solution NMR data of PCBM•**2'** also displayed complete desymmetrisation (Supplementary Figs. S69-S73).

The helicity of the apical Fe^{II} centre of PCBM•**2'** is again opposite to those of the basal Fe^{II} centres, as observed in the C_{60} adduct. The crystal structure shows that PCBM reacted with only one of the six anthracene panels on the opposite hemisphere to the original substituent, with the resulting adduct displaying the *trans*-3 substitution pattern[29]. The PCBM substituent disrupts the alignment of the diene units of the anthracene panels which form the fullerene-reactive sites (discussed fully in Supplementary Information Section 6), resulting in the observed differences in reactivity between C_{60} and PCBM.

Stereoselective di-substitution of fullerenes is a challenging problem. Past efforts have enabled the regioselective di-substitution of C_{60} through elegant masking strategies[21,22,38], but precise control over the absolute orientations of stereocentres has remained elusive, until now.

Retrieval of fullerene adducts

Taking advantage of the reversible nature of the imine bonds of the cages, we recovered the chiral aldehyde auxiliary *via* stepwise addition of tris(2-aminoethyl)amine (*tren*), releasing the covalently functionalised fullerene adducts (Fig. 2).

The gradual addition of *tren* (2 equiv) to a solution of C_{60}•**2** resulted in complete transformation to a new species C_{60}•**3** after 16 h at room temperature (Fig. 2a), which was separated from the mononuclear side-product Fe^{II}(tris(ethylimino-2-pyridyl)amine) *via* precipitation with toluene. The ^{1}H NMR spectrum of C_{60}•**3** (Supplementary Fig. S80) was consistent with removal of the apical metal centre and three of the twelve (*R*)-**A** residues incorporated in the periphery of cage C_{60}•**2**. ESI-MS further confirmed the identity of C_{60}•**3** as a partially disassembled "open" tetrahedral cage, with three basal Fe^{II} centres and three free amines. We infer the apical Fe^{II} to have been most readily removed due to increased strain introduced following the Diels-Alder reaction, and from the "mismatch" between (*R*)-**A** and the Δ configuration of the metal centre.

Further reaction of C_{60}•**3** with excess *tren* (5 equiv) produced a yellow precipitate after 48 h at 30 °C, which was isolated *via* centrifugation. Stepwise demetallation and disassembly of C_{60}•**2** with *tren* avoided the precipitation of partially disassembled cage products that occurred during direct reaction with 5 equiv of *tren,* thus increasing product yield and purity. Product ESI-MS and ^{1}H NMR spectra and were consistent with C_{60} adduct **4** (Fig. 4a) with three residues of **C** still attached.

The same procedure also allowed isolation of the other enantiomer of the C_{60} adduct **4**, starting from ΔΔΔΔ-**2**. The CD spectra of the enantiomers of **4** (Fig. 4b) are mirror images, as expected for mirror-image compounds. CD spectral features of the pair of enantiomers (Fig. 4b) agreed with those reported for *e,e,e* tris-adducts reported by Hirsch[32] and Nierengarten[41]. Analysis of both enantiomers of the purified **4** adduct *via* chiral stationary phase HPLC (Supplementary Fig. S89-90) revealed an *ee* of 87%.

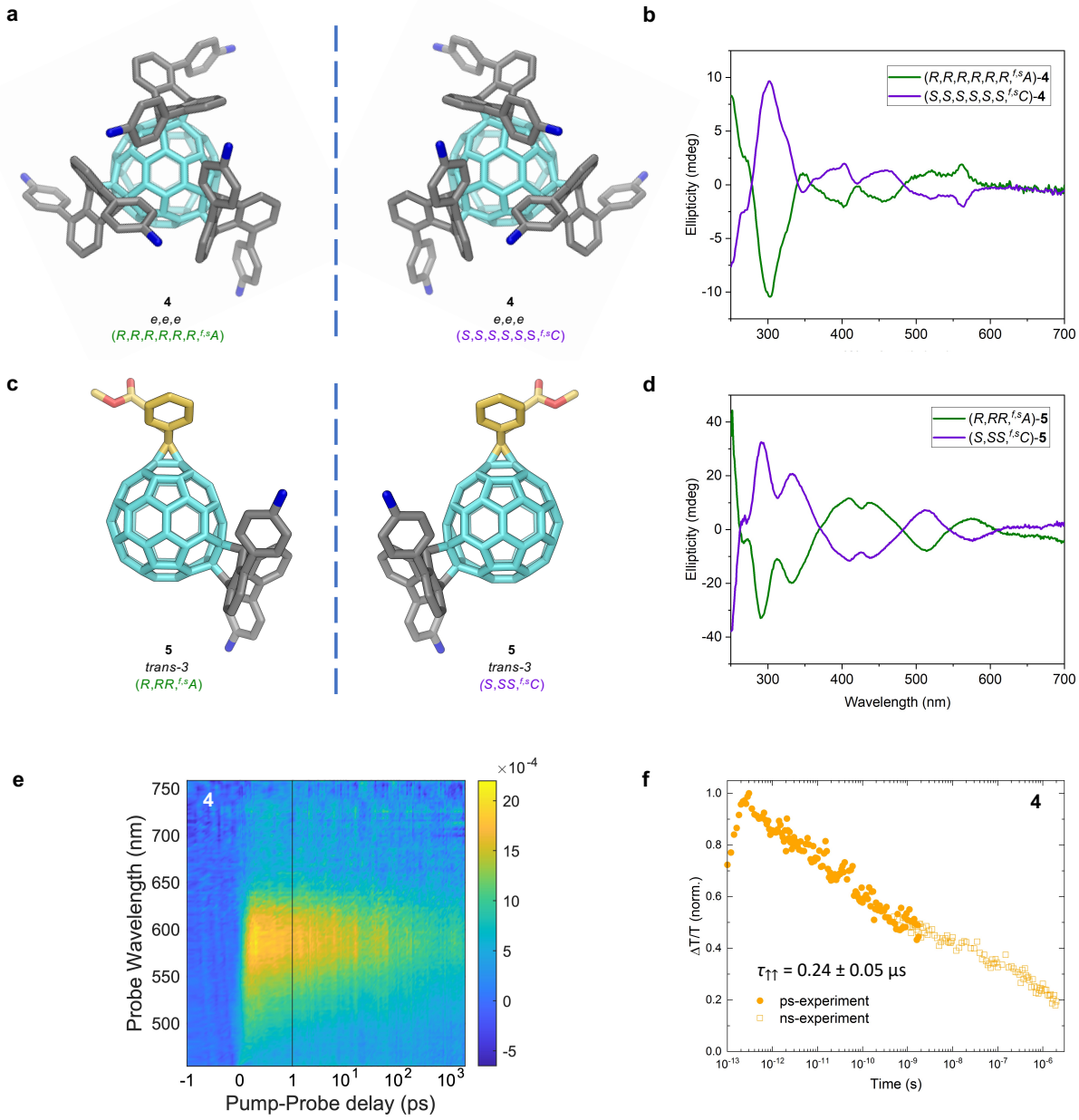

Fig. 4 | **Photophysics of retrieved fullerene adducts 4 and 5. a**, PM6-minimised models[42] of both enantiomers of **4**. **b**, CD spectra of both enantiomers of **4**. **c**, PM6 models of both enantiomers of **5**. **d**, CD spectra of both enantiomers of **5**. **e**, Transient absorption 2D pseudo-colour map of **4** excited at 400 nm with 100 fs pulses. **f**, Extracted excited-state kinetics spectrally integrated over 600-650 nm, yielding an effective lifetime of 0.24±0.05 µs indicative of a triplet state. Data at timescales longer than a ns were recorded using 355 nm excitation (see Supplementary Information Section 3 for details).

PCBM adduct **5** was also obtained from PCBM•**2** by treatment with *tren*, using the same procedure as described above for **4** (Fig. 2b). The preparation of **5** builds upon previous examples of hetero-functionalised adducts[21,40], achieving stereoselectivity as well as chemo- and regio-selectivity, which has proven challenging. The singly-demetalated intermediate PCBM•**3** (Fig. 4c) was also isolated following reaction

with 2 equiv of *tren*. Analysis of purified **5** *via* chiral HPLC revealed an *ee* of 64%, as compared to the 87% *ee* of **4**. The CD and UV-Vis spectra of both the enantioenriched *e,e,e* and *trans-3* adducts (see Fig. 4 and S84-85 and S96-97) were recorded. As expected, the enantiomers of **5** show mirror-image CD spectra (Fig. 4d). Both adducts show pronounced Cotton effects similar to those observed in other fullerene derivatives with chiral functionalization patterns[29].

We further studied the photophysics of fullerene adduct **4** using transient absorption (TA) spectroscopy (Figs. 4e, 4f), observing a long-lived excited state centred around 600 nm with an effective lifetime of 0.24±0.05 μs. This excited state lasts much longer than the typical radiative recombination rates of $S_0 \leftarrow S_1$ transitions for conjugated organic dyes (typically nanoseconds)[43]. We attribute the long lifetime observed here to the presence of triplet excitons, known to possess lifetimes of up to milliseconds, which formed rapidly within our instrument response time. In contrast to singlet states ($S = 0$), triplet states possess a net spin ($S = 1$). Notably, these efficiently generated triplets overlap spectrally with features observed in the CD spectrum (Fig. 4b). Interestingly, this could allow for the interaction of the triplet spins with the chirality of the structure *via* the chiral-induced spin-selectivity (CISS) effect[35,44] (see further discussion in Supplementary Information Section 3.3). While for **4** and **5** (see Supplementary Information Section 3 for TA data on **5**), the Diels-Alder cycloaddition of anthracene results in electronically-isolated benzene moieties, not energetically aligned to interact with the lower-lying fullerene states, future work will focus on the addition of functional groups with extended π-electron systems to tailor the photophysical properties of the adducts, or bestow upon them further functionalities, *e.g.* adding thiol groups to enable the formation of chiral self-assembled monolayers on gold electrodes[45], potentially enabling the creation of spin-optoelectronic devices such as polarised photodetectors[46], where a highly ordered film is crucial for achieving high efficiencies[47].

Conclusion

Chiral formylpyridine subcomponent **A** contributes to the growing supramolecular toolbox available for the construction of enantiopure metal-organic assemblies for chiral separations and guest molecule transformations. The point chirality of **A** transferred efficiently to the metal centres of cage **2**, which in turn imprinted its stereochemistry in traceless fashion upon the two chiral fullerene adducts **4** and **5**, which formed with high chemo-, enantio- and regio-selectivity. Chiral fullerene adducts with specific functionalization patterns were thus obtained directly in highly enantioenriched form without the need for time-consuming, iterative chromatographic separation, through the transfer of stereochemical information along an unbroken chain from subcomponent **A** to cage **2** and on to **4** and **5**, subsequent to the removal of the initial chiral aldehyde auxiliary. The selective preparations of cages **4** and **5** thus provide an initial proof-of-concept. Their structures also provide a starting point for the computational design[48] of specific new fullerene derivatives that might be produced in similar fashion, elucidating the way toward a potential methodology. The chiral fullerene adduct **4** was shown not only to exhibit circular dichroism, but also long exciton lifetimes assigned to triplets. These chiral fullerene adducts could therefore experience the CISS effect, and thus provide an interesting prospect to be used for generating spin polarisation in spin-valve devices[49], or as chiral electron transport layers for spinLEDs for more efficient displays and quantum information technologies[50].

Their high dissymmetry factors can also lead to applications as sensitive circularly polarised photodetectors, as has been recently demonstrated[27]. Their combination of chiroptical properties renders these adducts promising building blocks for chiral organic electronics.

The authors declare that all data supporting the findings of this study are included within the article and its Supplementary Information, and are also available from the authors upon request. Crystallographic data for the structures reported in this paper have been deposited at the Cambridge Crystallographic Data Centre, under the deposition numbers 24124135 (ΛΛΛΛ-**1**), 24124134 (ΔΛΛΛ-C_{60}•**2**) and 24124133 (PCBM•**2'**). Copies of these data can be obtained free of charge *via* www.ccdc.cam.ac.uk/data_request/cif.

Acknowledgements

This work was supported by the Engineering and Physical Sciences Research Council (EPSRC, EP/P027067/1) and the European Research Council (695009). Z.L. acknowledges the Cambridge Trust and China Scholarship Council for Ph.D. funding. A.W.H acknowledges Astex pharmaceuticals for post-doctoral funding. S.F. acknowledges funding from the Engineering and Physical Sciences Research Council (EPSRC, UK) through an EPSRC Doctoral Prize Fellowship. We thank Diamond Light Source for beamtime on Beamline I19 (CY21497). We also thank the Yusuf Hamied Department of Chemistry NMR facility for characterization data and Carles Fuertes-Espinosa for helpful discussion.

Author contributions

Z.L, T.K.R and J.R.N. conceived the study and wrote the manuscript. Z.L. performed the synthetic work with assistance from A.W.H. T.K.R. collected the X-ray data and refined the structures. N.V. and A.M. performed chiral HPLC studies on the fullerene adducts. S.F. carried out the transient absorption measurements. Z.L led the project overall. All the authors contributed to the manuscript preparation.

Additional information

Supplementary information is available in the online version of the paper. Reprints and permissions information is available online at www.nature.com/reprints. Publisher's note: Springer Nature remains neutral with regard to jurisdictional claims in published maps and institutional affiliations. Correspondence and requests for materials should be addressed to J.R.N.

Competing financial interests

The authors declare no competing financial interests.

References

1. Percec, V. *et al.* Steric Communication of Chiral Information Observed in Dendronized Polyacetylenes. *J. Am. Chem. Soc.* **128**, 16365–16372 (2006).
2. Clayden, J., Lund, A., Vallverdú, L. & Helliwell, M. Ultra-remote stereocontrol by conformational communication of information along a carbon chain. *Nature* **431**, 966–971 (2004).
3. Yashima, E. *et al.* Supramolecular Helical Systems: Helical Assemblies of Small Molecules, Foldamers, and Polymers with Chiral Amplification and Their Functions. *Chem. Rev.* **116**, 13752–13990 (2016).
4. Tsiamantas, C. *et al.* Selective Dynamic Assembly of Disulfide Macrocyclic Helical Foldamers with Remote Communication of Handedness. *Angew. Chem. Int. Ed.* **55**, 6848–6852 (2016).
5. Eelkema, R. *et al.* Nanomotor rotates microscale objects. *Nature* **440**, 163–163 (2006).
6. Han, B. *et al.* Asymmetric organocatalysis: an enabling technology for medicinal chemistry. *Chem. Soc. Rev.* **50**, 1522–1586 (2021).
7. Zhao, C. *et al.* Chiral Amide Directed Assembly of a Diastereo- and Enantiopure Supramolecular Host and its Application to Enantioselective Catalysis of Neutral Substrates. *J. Am. Chem. Soc.* **135**, 18802–18805 (2013).
8. Pan, M., Wu, K., Zhang, J.-H. & Su, C.-Y. Chiral metal–organic cages/containers (MOCs): From structural and stereochemical design to applications. *Coord. Chem. Rev.* **378**, 333–349 (2019).
9. Argent, S. P., Riis-Johannessen, T., Jeffery, J. C., Harding, L. P. & Ward, M. D. Diastereoselective formation and optical activity of an M_4L_6 cage complex. *Chem. Commun.* 4647–4649 (2005)
10. Castilla, A. M. *et al.* High-Fidelity Stereochemical Memory in a $Fe^{II}_4L_4$ Tetrahedral Capsule. *J. Am. Chem. Soc.* **135**, 17999–18006 (2013).
11. Nishioka, Y., Yamaguchi, T., Kawano, M. & Fujita, M. Asymmetric [2 + 2] Olefin Cross Photoaddition in a Self-Assembled Host with Remote Chiral Auxiliaries. *J. Am. Chem. Soc.* **130**, 8160–8161 (2008).
12. Mislow, K. & Siegel, J. Stereoisomerism and local chirality. *J. Am. Chem. Soc.* **106**, 3319–3328 (1984).
13. Howlader, P., Zangrando, E. & Mukherjee, P. S. Self-Assembly of Enantiopure Pd_{12} Tetrahedral Homochiral Nanocages with Tetrazole Linkers and Chiral Recognition. *J. Am. Chem. Soc.* **142**, 9070–9078 (2020).
14. Xuan, W., Zhang, M., Liu, Y., Chen, Z. & Cui, Y. A Chiral Quadruple-Stranded Helicate Cage for Enantioselective Recognition and Separation. *J. Am. Chem. Soc.* **134**, 6904–6907 (2012).
15. Brown, C. J., Bergman, R. G. & Raymond, K. N. Enantioselective Catalysis of the Aza-Cope Rearrangement by a Chiral Supramolecular Assembly. *J. Am. Chem. Soc.* **131**, 17530–17531 (2009).
16. Mahata, K., Frischmann, P. D. & Würthner, F. Giant Electroactive M_4L_6 Tetrahedral Host Self-Assembled with Fe(II) Vertices and Perylene Bisimide Dye Edges. *J. Am. Chem. Soc.* **135**, 15656–15661 (2013).

17. Kishi, N., Li, Z., Yoza, K., Akita, M. & Yoshizawa, M. An M_2L_4 Molecular Capsule with an Anthracene Shell: Encapsulation of Large Guests up to 1 nm. *J. Am. Chem. Soc.* **133**, 11438–11441 (2011).
18. Purba, P. C., Maity, M., Bhattacharyya, S. & Mukherjee, P. S. A Self-Assembled Palladium(II) Barrel for Binding of Fullerenes and Photosensitization Ability of the Fullerene-Encapsulated Barrel. *Angew. Chem. Int. Ed.* **60**, 14109–14116 (2021).
19. Nakamura, T., Ube, H., Miyake, R. & Shionoya, M. A C_{60}-Templated Tetrameric Porphyrin Barrel Complex *via* Zinc-Mediated Self-Assembly Utilizing Labile Capping Ligands. *J. Am. Chem. Soc.* **135**, 18790–18793 (2013).
20. Huang, N. *et al.* Tailor-Made Pyrazolide-Based Metal–Organic Frameworks for Selective Catalysis. *J. Am. Chem. Soc.* **140**, 6383–6390 (2018).
21. Fuertes-Espinosa, C. *et al.* Supramolecular Fullerene Sponges as Catalytic Masks for Regioselective Functionalization of C_{60}. *Chem* **6**, 169–186 (2020).
22. Ubasart, E. *et al.* A three-shell supramolecular complex enables the symmetry-mismatched chemo- and regioselective bis-functionalization of C_{60}. *Nat. Chem.* **13**, 420–427 (2021).
23. Chen, B., Holstein, J. J., Horiuchi, S., Hiller, W. G. & Clever, G. H. Pd(II) Coordination Sphere Engineering: Pyridine Cages, Quinoline Bowls, and Heteroleptic Pills Binding One or Two Fullerenes. *J. Am. Chem. Soc.* **141**, 8907–8913 (2019).
24. Leonhardt, V., Fimmel, S., Krause, A.-M. & Beuerle, F. A covalent organic cage compound acting as a supramolecular shadow mask for the regioselective functionalization of C60. *Chem. Sci.* **11**, 8409–8415 (2020).
25. Nishimura, T. *et al.* Macromolecular Helicity Induction on a Poly(phenylacetylene) with C_2-Symmetric Chiral [60]Fullerene-Bisadducts. *J. Am. Chem. Soc.* **126**, 11711–11717 (2004).
26. Bianco, A. *et al.* Synthesis, Chiroptical Properties, and Configurational Assignment of Fulleroproline Derivatives and Peptides. *J. Am. Chem. Soc.* **118**, 4072–4080 (1996).
27. Shi, W. *et al.* Fullerene Desymmetrization as a Means to Achieve Single-Enantiomer Electron Acceptors with Maximized Chiroptical Responsiveness. *Adv. Mater.* **33**, 2004115 (2021).
28. Fuertes-Espinosa, C., Pujals, M. & Ribas, X. Supramolecular Purification and Regioselective Functionalization of Fullerenes and Endohedral Metallofullerenes. *Chem* **6**, 3219–3262 (2020).
29. Thilgen, C. & Diederich, F. Structural Aspects of Fullerene Chemistry - A Journey through Fullerene Chirality. *Chem. Rev.* **106**, 5049–5135 (2006).
30. Riala, M. & Chronakis, N. A Facile Access to Enantiomerically Pure [60]Fullerene Bisadducts with the Inherently Chiral Trans-3 Addition Pattern. *Org. Lett.* **13**, 2844–2847 (2011).
31. Filippone, S., Maroto, E. E., Martín-Domenech, Á., Suarez, M. & Martín, N. An efficient approach to chiral fullerene derivatives by catalytic enantioselective 1,3-dipolar cycloadditions. *Nat. Chem.* **1**, 578–582 (2009).
32. Djojo, F. & Hirsch, A. Synthesis and Chiroptical Properties of Enantiomerically Pure Bis- and Trisadducts of C_{60} with an Inherent Chiral Addition Pattern. *Chem. – Eur. J.* **4**, 344–356 (1998).

33. Evans, D. A., Ennis, M. D. & Mathre, D. J. Asymmetric alkylation reactions of chiral imide enolates. A practical approach to the enantioselective synthesis of alpha-substituted carboxylic acid derivatives. *J. Am. Chem. Soc.* **104**, 1737–1739 (1982).
34. Bordoli, R. J. & Goldup, S. M. An Efficient Approach to Mechanically Planar Chiral Rotaxanes. *J. Am. Chem. Soc.* **136**, 4817–4820 (2014).
35. Naaman, R., Paltiel, Y. & Waldeck, D. H. Chiral molecules and the electron spin. *Nat. Rev. Chem.* **3**, 250–260 (2019).
36. Controlling the Transmission of Stereochemical Information through Space in Terphenyl-Edged Fe_4L_6 Cages. *J. Am. Chem. Soc.* **133**, 13652–13660 (2011).
37. Ousaka, N. *et al.* Efficient Long-Range Stereochemical Communication and Cooperative Effects in Self-Assembled Fe_4L_6 Cages. *J. Am. Chem. Soc.* **134**, 15528–15537 (2012).
38. Ronson, T. K., Pilgrim, B. S. & Nitschke, J. R. Pathway-Dependent Post-assembly Modification of an Anthracene-Edged $M^{II}_4L_6$ Tetrahedron. *J. Am. Chem. Soc.* **138**, 10417–10420 (2016).
39. Knof, U. & von Zelewsky, A. Predetermined Chirality at Metal Centers. *Angew. Chem. Int. Ed.* **38**, 302–322 (1999).
40. Xiao, Z., Geng, X., He, D., Jia, X. & Ding, L. Development of isomer-free fullerene bisadducts for efficient polymer solar cells. *Energy Environ. Sci.* **9**, 2114–2121 (2016).
41. Guerra, S., Schillinger, F., Sigwalt, D., Holler, M. & Nierengarten, J.-F. Synthesis of optically pure [60]fullerene e,e,e-tris adducts. *Chem. Commun.* **49**, 4752–4754 (2013).
42. Stewart, J. J. P. Optimization of parameters for semiempirical methods V: Modification of NDDO approximations and application to 70 elements. *J. Mol. Model.* **13**, 1173–1213 (2007).
43. In *Electronic Processes in Organic Semiconductors* I–XIII (John Wiley & Sons, Ltd, 2015). doi:10.1002/9783527685172.fmatter.
44. Naaman, R. & Waldeck, D. H. Spintronics and Chirality: Spin Selectivity in Electron Transport Through Chiral Molecules. *Annu. Rev. Phys. Chem.* **66**, 263–281 (2015).
45. Bain, C. D. & Whitesides, G. M. Molecular-Level Control over Surface Order in Self-Assembled Monolayer Films of Thiols on Gold. *Science* **240**, 62–63 (1988).
46. Yang, Y., da Costa, R. C., Fuchter, M. J. & Campbell, A. J. Circularly polarized light detection by a chiral organic semiconductor transistor. *Nat. Photonics* **7**, 634–638 (2013).
47. O'Neill, M. & Kelly, S. M. Ordered Materials for Organic Electronics and Photonics. *Adv. Mater.* **23**, 566–584 (2011).
48. Tarzia, A. & Jelfs, K. E. Unlocking the computational design of metal–organic cages. *Chem. Commun.* **58**, 3717–3730 (2022).
49. Nguyen, T. D., Ehrenfreund, E. & Vardeny, Z. V. Spin-Polarized Light-Emitting Diode Based on an Organic Bipolar Spin Valve. *Science* **337**, 204–209 (2012).
50. Kim, Y.-H. *et al.* Chiral-induced spin selectivity enables a room-temperature spin light-emitting diode. *Science* **371**, 1129–1133 (2021).